The Impact of Donor-Orientation on the Emission Properties of Chlorinated Trityl Radicals

Mona E. Arnold[1†], Robert Toews[2†], Lars Schneider[3†], Jonas Schmid[1], Miftahussurur Hamidi Putra[4], Michael Busch[5,6], Axel Groß[4,7], Felix Deschler,[3]* Andreas Köhn[2]*, and Alexander J. C. Kuehne[1]*

[1]Institute of Organic and Macromolecular Chemistry, Ulm University, Albert-Einstein-Allee 11, 89081 Ulm, Germany.

[2]Institute for Theoretical Chemistry, University of Stuttgart, Pfaffenwaldring 55, 70569 Stuttgart, Germany.

[3]Institute of Physical Chemistry, University of Heidelberg, Im Neuenheimer Feld 229, 69120 Heidelberg, Germany.

[4]Institute of Theoretical Chemistry, Ulm University, Oberberghof 7, 89069 Ulm, Germany.

[5]Division of Materials Science, Department of Engineering Sciences and Mathematics, Luleå University of Technology, 971 87 Luleå, Sweden.

[6]Wallenberg Initiative Materials Science for Sustainability (WISE), Luleå University of Technology, 971 87 Luleå, Sweden.

[7]Helmholtz Institute Ulm (HIU) for Electrochemical Energy Storage, Helmholtzstraße 11, 89081 Ulm, Germany.

ABSTRACT: Chlorinated trityl radicals functionalized with electron-donating groups are promising red-emitting materials for optoelectronic and spintronic applications, overcoming the spin-statistical limit of conventional emitters. Donor functionalization induces charge transfer character, enhancing photoluminescence quantum yield, which depends on the donor strength and its orientation. However, donor functionalized tris(trichlorophenyl)methyl radicals show lower quantum yield than their perchlorinated derivatives, likely due to weaker donor-acceptor electronic coupling and enhanced non-radiative decay. We present a novel trityl derivative with two additional chlorines that restrict the orientation of the donor to a nearly perpendicular arrangement towards the trityl plane, minimizing vibronic coupling and non-radiative losses. Spectroscopic and computational studies reveal that this steric constraint improves the photoluminescence quantum yield compared to the tris(trichlorophenyl)methyl analogues. These findings highlight the potential of donor-acceptor decoupling to enable efficient, red-shifted emission, offering a design strategy for high-performance radical emitters.

KEYWORDS: *light emitting radicals, triaryl methyl radicals, TTM, transient absorption spectroscopy, DFT*

INTRODUCTION

Stable, chlorinated trityl radicals functionalized with electron donating units represent promising candidates as efficient red-emitters for organic light-emitting diodes. Since triplet states are not available in radical emitters and emission occurs from doublet states upon electrical excitation, the spin-statistical limitation of conventional emitters to 25 % internal quantum efficiency is lifted in radical emitters.[1–6] Typically, chlorinated trityl radicals exhibit only low photoluminescence quantum yield ϕ_{PL}, because the relevant transitions are symmetry-forbidden. However, the emission performance can be improved by appropriate functionalization with electron-donating groups, evoking symmetry breaking and a charge transfer (CT) excited state.[7–11] Both, the emission wavelengths λ_{max} and ϕ_{PL} depend highly on the electron-donating strength of the substituent.[12] Moreover, the structural arrangement of the donor relative to the trityl radical appears to have a significant impact on the emission characteristics, exemplified by the comparison of trityl radical functionalized with triphenylamine (TPA), 3-phenylcarbazole (3PCz) and phenyl-*N*-carbazole (PCz). Interestingly, the three donors all exhibit a triphenylamine scaffold, in which a bond between two phenyl rings evokes a planarized carbazole unit in case of the 3PCz an PCz units. This planarization leads to significant differences in the trityl emission efficiency. More interestingly, when attaching the same donor to the tris(trichlorophenyl)methyl radical (TTM) or the perchlorinated trityl radical (PTM), the TTM analogues exhibit lower ϕ_{PL} than the PTM derivatives, while the underlying reasons have not been elucidated yet.[1,13,14] The obvious difference between the TTM and PTM derivatives is the disparate acceptor strength induced by the higher number of chlorine substituents in the PTM. Moreover, the added chlorine substituents in PTM may restrict the rotation and the orientation of the donor towards the trityl radical plane. The suppression of geometric differences in the ground and excited state favors efficient emission by minimizing non-radiative relaxation.[15,16] A smaller

dihedral angle between donor and the trityl plane ($\measuredangle_{DA}$) has been suggested to lead to enhanced electronic coupling between the donor and the trityl orbitals, leading to more efficient emission.[13] However, this is in contrast to the experimentally observed ϕ_{PL} of donor functionalized TTM radicals, which are much lower compared to the PTM homologues.

A recent report has shown that high ϕ_{PL} in donor functionalized TTM radicals can be explained by the absence of high-frequency vibrations, for example carbon-carbon stretching modes that could couple to the first excited doublet state (D_1) and lead to its non-radiative relaxation.[17] In trityl radicals the D_1 is typically described as a charge transfer (CT) state.[7,15,18,19] The higher the vibrational frequency coupling to the CT exciton, the more likely becomes vibrational deactivation leading to high non-radiative recombination rates. Higher-lying excited states (D_2 and above) in donor functionalized trityl radicals are accessible by excitation in the blue and UV spectral region. These higher excited states exhibit significant locally excited (LE) state character and can accommodate high-frequency vibrations.[17] While higher excited states in donor-functionalized trityl radicals typically relax quickly to the D_1 state, vibrational coupling occurs on timescales that can compete with internal conversion. Therefore, such vibronic effects in higher excited states could contribute to non-radiative relaxation. If the LE character in light-emitting trityl radicals could be reduced, to avoid coupling to high-frequency modes located on the trityl site, then, it would be possible to further improve the emission characteristics of donor functionalized trityl radicals. Electronic decoupling of the donor and acceptor moieties has been demonstrated to suppress non-radiative relaxation in a series of donor-functionalized PTM radicals.[19] This concept would also allow to overcome the restrictions of the energy gap law and achieve high ϕ_{PL} for emission that is strongly red-shifted into the near IR spectrum. However, to date, there is no study that independently investigates the effect of steric restriction of the donor rotation to produce clear CT excited states on the emission performance.

Here, we introduce a new trityl derivative (TBTM) carrying only two additional chlorine atoms on the phenyl ring connected to the donor, to systematically study the impact of donor orientation without significantly changing the electronic properties and acceptor strength of the trityl radical moiety. While the electron-accepting strength of the radical moiety is only slightly modified compared to TTM, we show that the additional chlorines restrict the orientation of the donor to almost perpendicular with respect to the TBTM plane. We employ spectroscopy and quantum chemical calculations to explain the improved emission characteristics of the TBTM compared to the TTM derivatives, enabling the rational design of future high-performance radical emitters.

RESULTS AND DISCUSSION

Synthesis

We start by preparing the new unsymmetrically chlorinated TBTM (2,3,5,6-tetrachlorophenyl)bis(1,3,5-trichlorobenzene) methyl radical precursor (**1**). First, 3-bromo-1,2,4,5-tetrachlorobenzene is alkylated using chloroform to give the halogenated benzyl derivative **2**. The latter is then used in a subsequent Friedel-Crafts alkylation to give the unsymmetrically chlorinated triphenyl methane **1** in excellent overall yield. The *para*-bromide functionality allows efficient Suzuki cross-coupling of the respective electron donors (PCz, 3PCz, TPA).

Fortunately, the steric hindrance caused by the chlorine atoms in the *meta*-position does not lower the reactivity of the bromide site in **1**, allowing donor functionalization in good to excellent yields at mild conditions (see Figure 1). The corresponding donor-functionalized TBTM radicals are obtained following the established deprotonation-oxidation protocol.[7,13,20,21] Deprotonation of the α-carbon using potassium *tert*-butoxide is followed by mild oxidation of the carbanion to the radical using *p*-chloranil. The open-shell nature of the resulting compounds is confirmed by EPR spectroscopy (see Figure S2).

Additionally, we synthesize the TTM series carrying the respective donors for a direct comparison (see Figure 1). For this series of TTM-TPA, TTM-3PCz, and TTM-PCz radicals, we develop slightly adapted reaction procedures inspired by synthetic protocols from the literature.[13,14] In contrast to previously reported procedures starting from HTTM,[20] our method delivers improved yields of 49 % for TTM-TPA, 80 % for TTM-3PCz, and 93 % for TTM-PCz (see the Supporting Information for experimental details).[13,17]

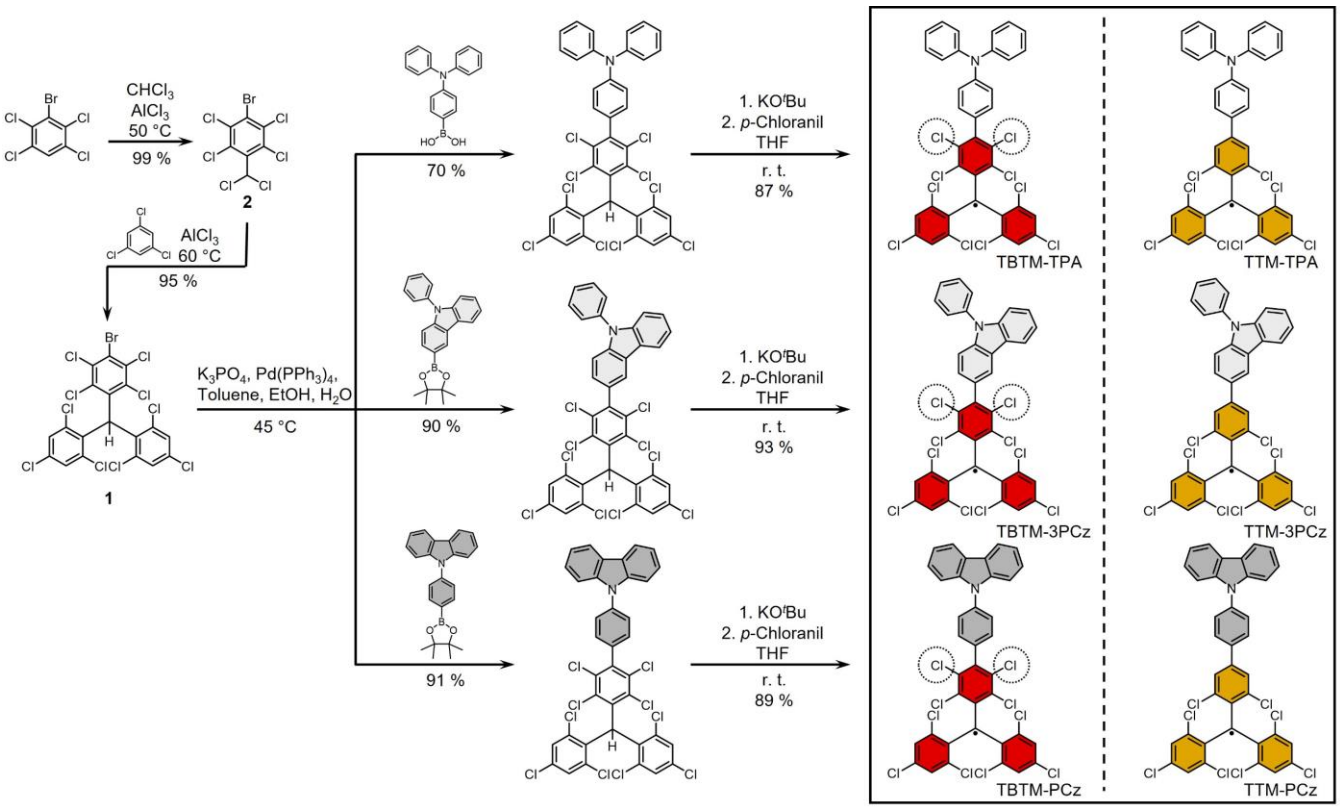

Figure 1: Synthesis of new donor-functionalized TBTM trityl radicals carrying eight chlorine atoms. The unsymmetric precursor for Suzuki coupling **1** is obtained from a two-step Friedel-Crafts alkylation reaction. TTM derivatives with identical donors are shown for comparison.

Analysis of the excited state characteristics

We characterize our donor-functionalized radicals using UV-vis spectroscopy. To avoid strong interactions of the radicals in the excited state with the solvent, we choose cyclohexane as a suitable non-polar solvent. When we compare the UV-vis absorption spectra of our TBTM and TTM derivatives, we observe characteristic features of trityl radicals, including strong absorption in the UV and a weak band in the visible region, typically associated with the $D_0 \rightarrow D_1$ transition (see Figure 2). The strong absorption in the UV is insensitive to the donor substitution, substantiating the LE character of the higher-energy transition (see Figure 2). By contrast, the $D_0 \rightarrow D_1$ absorption at lower energy undergoes a red-shift from PCz to 3PCz and TPA, correlating with the donor strength and indicating the increasing CT character of the transition with increasing donor strength (see Figure 2 and Table 1). This bathochromic shift with increasing donor strength is in agreement with prior reports for donor-functionalized TTM and PTM derivatives.[12,19] This bathochromic shift can be rationalized by an increased stabilization as the CT character of the excited state becomes more pronounced. Notably, the extinction coefficients ε for the $D_0 \rightarrow D_1$ transitions are reduced in the TBTM series with respect to the TTM series (see Figure 2 and Table 1). This reduction in ε indicates diminished electronic coupling between donor and trityl units in the donor functionalized TBTM radicals compared to the TTM series. Presumably, a larger dihedral angle ($\measuredangle_{DA}$) between donor and trityl radical in the TBTM series, due to the steric constrains of the *meta*-chlorides (*ortho* to the donor moieties) could be the reason for the weakened electronic coupling.

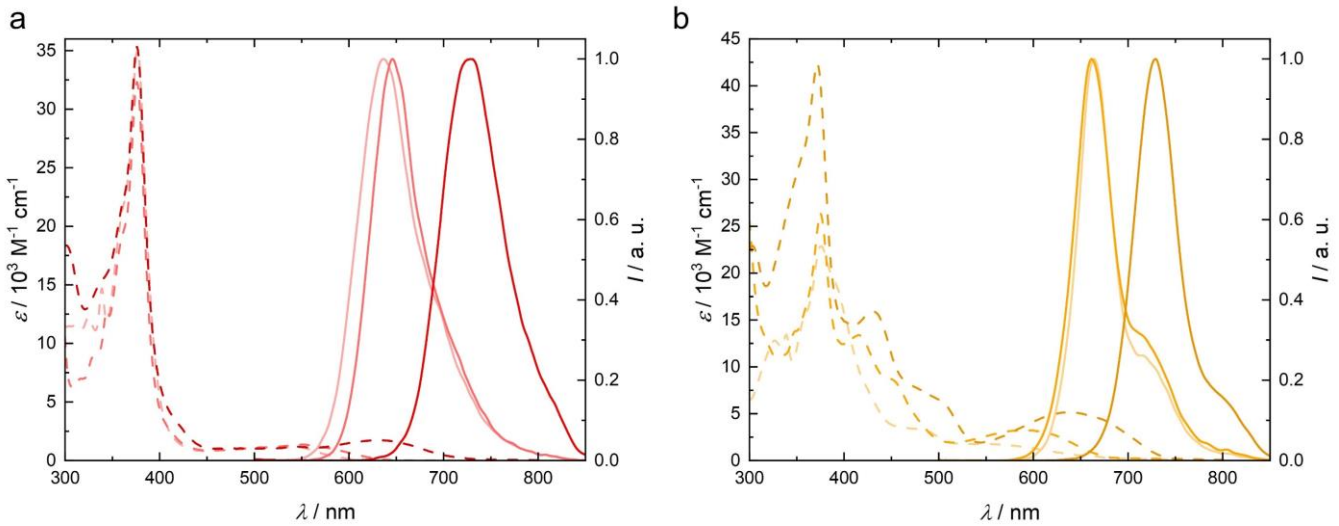

Figure 2: Absorption (dashed lines) and emission (solid lines) spectra measured for cyclohexane solutions (10^{-4} M) of a) TBTM (red) and b) TTM (orange), functionalized with TPA (dark color), 3PCz (medium color), and PCz (light color).

To gain further insight into the geometry and the transitions of the donor functionalized TBTM and TTM radical series, we perform time-dependent density functional theory (TD-DFT) calculations at the CAM-B3LYP, def22-SVP level of theory (see SI for computational details).[22] We optimize the molecules in their ground state geometry to determine $\measuredangle_{DA}$(GS). As expected, we find large dihedral angles $\measuredangle_{DA}$(GS) = 70° – 90° for the TBTM series, while the TTM derived radicals shows significantly smaller $\measuredangle_{DA}$(GS) = 31° – 33° (see Figure 3a and Table 1). Apparently, the additional *meta*-chloride groups in TBTM induce indeed sufficient steric hindrance to enforce a much larger dihedral angle between donor and acceptor compared to TTM.

Table 1: Photophysical properties for cyclohexane solutions of TBTM and TTM, functionalized with identical substituents, dihedral angles $\measuredangle_{DA}$ between donor and trityl moieties of the radicals in their ground and excited state geometry obtained from (TD-)DFT calculations, and norms of the non-adiabatic coupling vectors $|D^{(01)}|$ for the D_0 and D_1 state and $|D^{(12)}|$ for the D_1 and D_2 state. [a] Values adopted from ref. [13].

Compound	λ_{abs} / nm	ε (D_0-D_1) / 10^3 M^{-1} cm^{-1}	λ_{em} / nm	ϕ / %	τ / ns	k_r / 10^6 s^{-1}	k_{nr} / 10^6 s^{-1}	$\measuredangle_{DA}$ (GS) / °	$\measuredangle_{DA}$ (ES) / °	$\lvert\boldsymbol{D}^{(01)}\rvert$ / cm^{-1}	$\lvert\boldsymbol{D}^{(12)}\rvert$ / cm^{-1}
TBTM-TPA	630	1.73	729	43	17.1	25.1	33.3	70	65	29	76
TBTM-3PCz	548	1.37	646	59	27.3	21.2	15.4	72	53	45	568
TBTM-PCz	543	1.15	636	16	12.7	12.6	66.1	90	90	6	76
TTM-TPA	635	5.14	729	12	6.4	18.8	15.0	31	12	70	116
TTM-3PCz	593	3.25[a]	664	27	15.7	14.6	49.0	32	13	80	283
TTM-PCz	545	1.82[a]	662	4	4.6	8.7	208.7	33	8	71	330

We also compute the excited state (D_1) geometry on the CAM-B3LYP (γ = 0.098 a_0^{-1}), def2-SVP level, and we find that the donor substituents tend to rotate into the trityl plane upon excitation. For the TBTM series the change in dihedral angle is typically smaller than for the TTM series. In addition, the resulting dihedral angles in the excited state are larger for the TBTM ($\measuredangle_{DA}$(ES) = 53 – 90°) than for the TTM ($\measuredangle_{DA}$(ES) = 8 – 13°) derivatives (cf. Table 1).

We calculate the natural transition orbitals (NTOs) for the $D_0 \rightarrow D_1$ transition to learn whether the transition has more LE or CT character (see Figure 3b and c). For all molecules under investigation the electron NTO is located on the trityl moiety, whereas the hole NTO remains on the donor unit. However, for the TBTM radical series, we

observe a much more stringent charge separation, whereas the TTM series is characterized by substantial overlap between electron and hole NTOs, rendering the transition state more hybridized with contribution from a locally excited and a charge transfer state (HLCT).[3,8,23] These observations align well with our experimental results, corroborating the stronger CT character for the TBTM radicals and the HLCT behavior for the TTM series. The spectra of the TTM radicals show a series of absorption events between 400 and 500 nm in addition to the above-discussed bands, which are absent in TBTM (see Figure 2). These bands result from transitions to higher-lying excited states with significantly smaller oscillator strength in the TBTM compared to the TTM series. The diminished transition probability is reasonable when considering that the higher-lying excited states will involve orbitals on both donor and acceptor moieties, which will be more decoupled for the TBTM radicals with more perpendicular donor to trityl planes. Thus, the UV-vis spectra of the TBTM series consist only of the features of the isolated donor and acceptor species, apart from the $D_0 \rightarrow D_1$ transition (see Figure 2).

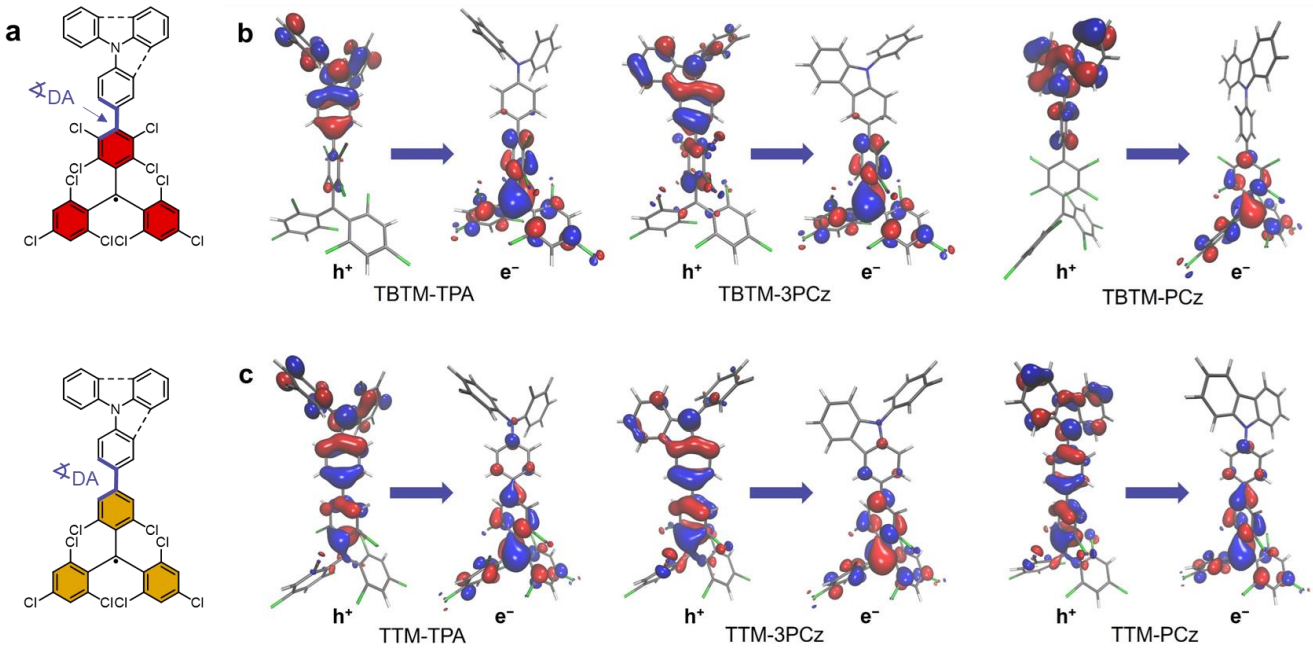

Figure 3: (a) Chemical structure of TTM and TBTM derivatives with the connection between donor and acceptor, defining the dihedral angle $\measuredangle_{DA}$ highlighted in blue. Hole (h^+) and electron (e^-) natural transition orbitals for the $D_0 \rightarrow D_1$ transition in (b) TBTM, and (c) TTM, both functionalized with TPA, 3PCz, and PCz electron donors in their ground state geometries, calculated using CAM-B3LYP, (γ = 0.098 a_0^{-1}) def2-SVP. The respective sign of the wave function is indicated in blue (−) and red (+).

Character of the excited state and the transitions to the ground state

When we compare the photoluminescence spectra of the TBTM derivatives to the TTM series, we observe that the spectra are less structured for the TBTM with less resolved vibrational features than for TTM, while the spectra are equally broad. Presumably, coupling to vibrational modes appears with higher disorder and the lifetimes of the modes are shorter resulting in broadening of the signal. The emission of TBTM-PCz and TBTM-3PCz is blue-shifted compared to their TTM homologues. This hypsochromic shift can be explained by the reduced delocalization of the hole and electron in the D_1 state compared to the TTM radicals.

We determine ϕ_{PL} of the donor functionalized TBTM and TTM radicals in cyclohexane (see Table 1). ϕ_{PL} is drastically increased for the donor functionalized TBTM radicals compared to the TTM series, with a maximum ϕ_{PL} of 59 % for TBTM-3PCz (see Table 1). We have previously shown that the donor strength of the substituent needs to be adjusted to the electron-accepting capability of the radical moiety to ensure maximum emission efficiency by suppression of non-radiative decay pathways.[12] TBTM will be a slightly stronger acceptor than TTM for the larger number of electron-withdrawing chlorine atoms. Therefore, the increase in ϕ_{PL} could also be an effect of the more

balanced donor acceptor combination. Apart from adjusting the donor strength, the CT character of the excited state can also be tuned by the solvent polarity. More polar solvents are expected to stabilize the CT state and favor intramolecular charge migration. Indeed, we find ϕ_{PL} of TBTM-PCz to be increased from 16 to 34 %, when changing the solvent to slightly more polar toluene. By contrast, TBTM-TPA and TTM-TPA exhibit identical emission maxima λ_{em} of 729 nm, whereas the ϕ_{PL} value is greatly increased for TBTM-TPA (43 %) versus TTM-TPA (12 %) (see Table 1). Therefore, we hypothesize that the increase in ϕ_{PL} is related to the reduced LE character and restricted rotation around the bond between donor and trityl acceptor.

Huang Rhys factors

To gain insight into the level of steric hindrance of the rotation of the donor moieties against the trityl plane, we compute the Huang-Rhys (HR) factors for the $D_0 \rightarrow D_1$ transition in the lower energy frequency domain, representing the torsional modes.[24] In the TTM series, we observe strong HR factors for frequencies around 210 cm^{-1}, typical for torsional modes (see Figure S6 and Figure S7 for illustration of the modes). Interestingly, these modes are absent or weakened in the donor functionalized TBTM series, confirming that the additional chlorine atoms indeed provide sufficient steric hindrance to inhibit the torsional modes of the donor against the trityl plane (cf. Figure 3 with Figures S6 and S7).

To obtain a mechanistic understanding of our systems, we apply a semi-quantitative analysis based on the expression

$$k_{m\rightarrow n} = \frac{\pi}{\hbar} \sum_{\substack{\mu \\ D_\mu^{(mn)} \neq 0}} \left| D_\mu^{(mn)} \right|^2 \sum_{\nu} \prod_{\substack{\mu \\ S_\mu \neq 0}} \left| \left\langle \phi_\mu^{(m\nu)} \middle| \phi_\mu^{(n0)} \right\rangle \right|^2 \delta\left(E_n - E_m - \sum_\sigma \hbar\omega_\sigma \right) \quad (1)$$

of the rate constant for non-radiative decay.[25,26] The first summation in equation (1) contains the projection $D_\mu^{(mn)}$ of the non-adiabatic coupling vector between the electronic states m and n on the normal mode μ:

$$D_\mu^{(mn)} = \hbar\omega_\mu \left\langle \psi_\mu^{(m)} \middle| \frac{\partial}{\partial Q_\mu} \middle| \psi_\mu^{(n)} \right\rangle, \quad (2)$$

where ω_μ and Q_μ are the angular frequency and normal coordinate of the mode μ, and $\psi_\mu^{(l)}$ the electronic wave function of the state l evaluated at Q_μ. The second summation in equation (1) can be recognized as the energy-shifted and Franck-Condon weighted density of states (FCWD) with $\phi_\mu^{(l\mu)}$ as the wave function of the mode μ within the vibrational state v and the electronic state l, E_l as the adiabatic energy of the electronic state l and δ as the Dirac delta function.[26] The quantity S_μ is the HR factor of the mode μ and represents a measure for exciton-phonon coupling. In section 3.4 of the Supporting Information, we give a more detailed account on the HR factor and its influence on the rate constant $k_{m\rightarrow n}$, and discuss the assumptions involved in our approach. Here, we stress that the HR factors significantly contribute to the FCWD and that HR factors related to high-frequency modes are considered to promote fast non-radiative decay.[17,27] Therefore, we can obtain a semi-quantitative understanding of the non-radiative decay in our systems by considering non-adiabatic and exciton-phonon coupling for the first excited state.

When calculating the HR factor for the $D_0 \rightarrow D_1$ transition in the high-frequency range from 1000 to 1700 cm^{-1}, we observe only weak vibrational coupling to the exciton for both, the donor-functionalized TTM and the TBTM radicals (see Figure S8). The strongest mode close to 1600 cm^{-1} is present in all TTM-based radicals and has previously been detected in computational Huang-Rhys factor analysis and experimentally by excited state vibrational spectroscopy in TTM-TPA.[17,19] This mode has been identified as a C-C and C-H breathing mode of the phenyl rings in the trityl moiety.[15,17] This breathing mode can couple to the exciton and can cause non-radiative decay. Beneficially for high values of ϕ_{PL}, this mode is suppressed in our TBTM radical series (see Figure S8). However, the HR factors are generally too small to explain the pronounced difference of the ϕ_{PL} values of the different series.

Donor-acceptor systems based on a functionalized trityl moiety can exhibit electronic-state hybridization between the D_1 state and the D_2 state, where the D_1 state typically bears CT character and the D_2 state is a dark LE state.[23,28] If hybridization becomes relevant, the expression for $k_{1\rightarrow 0}$ in equation (1) needs to be extended beyond the two-

state model as to include contributions from the D_2 state (see Figure S10 for $D_0 \rightarrow D_2$ NTOs and section 3.2 of the Supporting Information for details). In our analysis, we account for these potential contributions by also considering the non-adiabatic coupling vector between the first two excited states and the HR factors related to the D_2 state. Please note that our semi-quantitative approach mainly allows for the comparison between a TBTM system and its TTM analogue and thus for an understanding of the alteration of non-radiative decay upon additional chlorination. We can understand the non-radiative decay in our systems in terms of the non-adiabatic coupling vectors $D^{(mn)}$ between the electronic states m and n, and the HR factors S_μ. The norms of the coupling vectors $D^{(01)}$ and $D^{(12)}$ for the TTM and TBTM series are listed in Table 1. It becomes obvious that in every case the coupling between the D_1 and D_2 state is considerably larger than the coupling between the D_1 state and the ground state D_0. This implies an electronic hybridization between the first two excited states in all systems. Thus, the exciton-phonon coupling in the D_2 state influences the non-radiative rate constant $k_{1\rightarrow0}$. For TBTM-PCz and TBTM-TPA, the norms for $D^{(01)}$ and $D^{(12)}$ are consistently smaller than for the TTM analogues. The diminished CT-LE hybridization suppresses non-radiative relaxation, which agrees well with the experimentally observed trend of improved ϕ_{PL} for the TBTM series. Qualitatively, the reduced non-adiabatic couplings can be understood in terms of the Mulliken-Hush approach, where the coupling between two electronic states is approximately inversely proportional to the change in molecular dipole moment.[29] Hence, the decreased coupling for TBTM-PCz and TBTM-TPA can be linked to the marked CT character in the D_1 state. Obviously, the close-to-perpendicular orientation of donor and acceptor units in the TBTM series induces pronounced charge-separation and thus hinders the hybridization of CT and LE states due to a lack of orbital overlap.

In contrast to the other two TBTM derivatives, for TBTM-3PCz we observe a pronounced coupling between the D_1 and D_2 state, which is even increased with respect to the TTM analogue (see Table 1). Despite this strong coupling, which is considered to favor non-radiative decay, TBTM-3PCz still shows improved ϕ_{PL} when compared to TTM-3PCz. This experimental observation can be rationalized by the altered exciton-phonon coupling of the D_2 state. For the case of significant CT-LE hybridization the HR factors of this state give insights into non-radiative relaxation. For the TTM series, we observe three vibrational modes in the higher frequency domain that strongly couple to the D_2 excited state (see Figure 4). By contrast, in the TBTM series the HR factors of these modes are diminished.

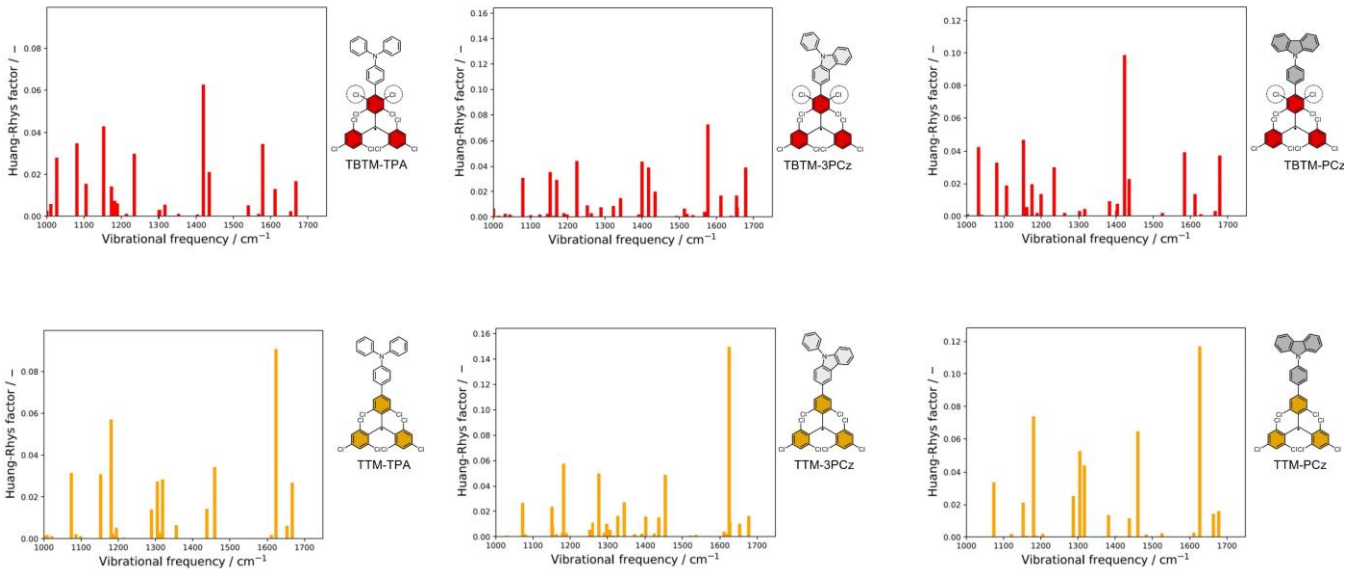

Figure 4: Huang-Rhys factors for the D_2 states in the high-frequency domain as a measure for exciton-phonon coupling (TBTM: red, TTM: orange). Due to considerable electronic hybridization between the D_1 and D_2 states, the HR factors in the D_2 state influence non-radiative decay. Calculations performed on the CAM-B3LYP/def2-SVP level of theory.

The modes around 1185 cm^{-1} partly extend to the donor fragment, whereas the other two modes are primarily confined to the TTM moiety (see Figure S9). Especially in the frequency region of these two modes, exciton-

phonon coupling of the TBTM systems is either suppressed or absent. This behavior can be explained by recalling the enhanced CT character of the D_1 state in all TBTM systems. It follows that the spatial separation between hole and particle orbitals for the transition between D_0 and D_1 state is increased, which is shown to suppress non-radiative deactivation pathways.[17] Therefore, we can understand the improved non-radiative rate constants of TBTM-PCz and TBTM-TPA by a combined effect of reduced non-adiabatic coupling and suppressed exciton-phonon coupling in the D_2 state. For TBTM-3PCz, ϕ_{PL} is improved compared to TTM-3PCz despite the comparatively strong non-adiabatic coupling between the D_1 and D_2 state. The decreased coupling to high-frequency modes in both the D_1 and D_2 excited states allows for the efficient suppression of non-radiative relaxation.

Time-resolved spectroscopy

The reduction of non-adiabatic and exciton-phonon coupling in the donor functionalized TBTM radicals versus the TTM derivatives is confirmed, when we probe our molecules by transient absorption (TA) spectroscopy. We take a closer look at the TPA-donor functionalized trityl radicals, since both types of TTM and TBTM radicals delivered similar emission spectra, despite the much greater ϕ_{PL} in the TBTM-TPA derivative (cf. Figure 2 and Table 1). The TA spectra for the other PCz and 3PCz functionalized TBTM and TTM radicals exhibit the same qualitative effects and are therefore shown in the Supporting Information in Figures S11 – S16.

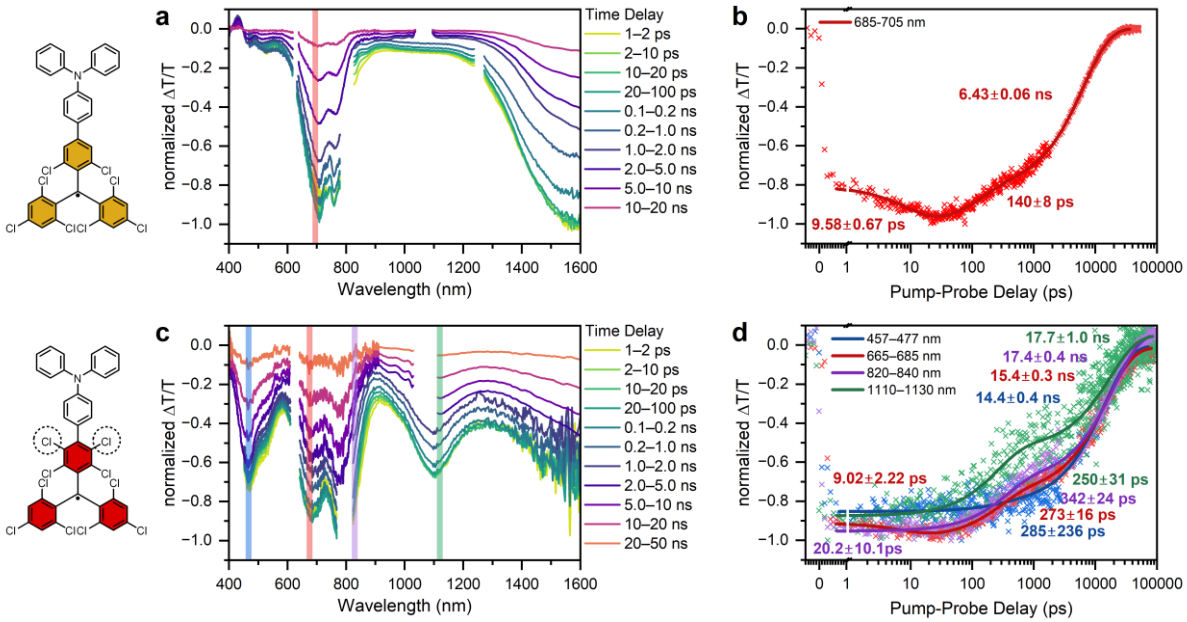

Figure 5: Normalized transient absorption spectra at time delays as indicated (a&c) and kinetic (b&d) of compounds TTM-TPA and TTBM-TPA dissolved in cyclohexane upon excitation at 630 nm. Gaps in the spectra are due to the laser fundamentals.

The dynamics of the photoexcited state populations in the TTM and TBTM derivatives are investigated in cyclohexane solution by excitation to the D_1 state by pumping at λ_{ex} = 630 nm for the TPA-derivatives (and λ_{ex} = 550 nm for the PCz and 3PCz-derivatives), as well as into a higher locally excited state by pumping at λ_{ex} = 375 nm, resonant with the observed UV-vis maxima (cf. Figure 2) (see section 4 in the Supporting Information for a detailed experimental description). TTM-TPA shows one strong excited state absorption (ESA) band between 600 – 900 nm, split into a double peak by the stimulated emission around 720 nm (see Figure 5a). This ESA transition can be assigned to the $D_1 \rightarrow D_2$ excitation. A secondary ESA feature is observed at 1600 nm (see Figure 5a). For TBTM-TPA, three bands with enhanced intensities appear (see Figure 5c). The band between 600 – 750 nm is again assigned to the $D_1 \rightarrow D_2$ excitation. The two new bands at 460 nm and 800 nm are assigned to the TBTM anion and triphenylamine radical cation, respectively, of the CT state, based on spectro-electrochemical TA spectroscopy of triarylamine-donor functionalized trityl radicals reported in the literature.[19,30] The separation of these two bands indicates strong

electronic decoupling of the donor and acceptor unit, further corroborating their close-to-perpendicular orientation. A further excited state absorption band appearing at 1100 nm is likely related to this enhanced CT character. Similar to TBTM-TPA, new bands appear for the PCz- and 3PCz-substituted TBTMs at 450 nm and 850 nm (see Figures S14 and S16).

The ESA features of both TTM-TPA and TBTM-TPA show a similar rise time after excitation (within our time resolution). By contrast, the decay times are extended for the TBTM-derivative (cf. Figure 5b and d). Their longest excited state lifetimes, as determined by biexponential fits to the TA spectroscopy data (6.43 ns for TTM-TPA and 14.4 – 17.7 ns for TBTM-TPA), match the photoluminescence lifetimes τ determined by transient photoluminescence (6.4 ns for TTM-TPA and 17.1 ns for TBTM-TPA) (cf. Figures 5b and 5d with Figures S17 and Table 1). Both spectroscopic techniques confirm that the excited D_1 state decays much faster in TTM-TPA than in TBTM-TPA. The increased excited state lifetime in TBTM-TPA combined with the higher ϕ_{PL} indicates that there are fewer non-radiative decay pathways, compared to the TTM-TPA radical. The TA spectra of the other donor functionalized radicals lead to the same conclusions (see Figure S13 and S16). The reduction of torsional and breathing modes in the TBTM radicals compared to the TTM series, as indicated in the Huang-Rhys analysis, will be responsible for this improved excited state lifetime in the donor functionalized TBTM radicals.

Interestingly, the TA spectra show also population of the D_1 state after excitation with the λ_{ex} = 375 nm laser into higher excited states (see Figure S11 to S16). The respective signal for the D_1 population increases over the course of the first 1000 ps, indicating that the state becomes further populated by slowly-relaxing higher excited states (see b panels in Figures S11 – S16). We see matching kinetics for TBTM-TPA, indicating that the relaxation rates from higher excited states are comparable in donor functionalized TBTM and TTM radicals. These results indicate that the higher excited states (D_2 and higher) decay into the D_1 state on a timescale that is consistent with internal conversion.

We use the determined lifetimes τ of the D_1 state to determine the rate constants for radiative (k_r) and non-radiative (k_{nr}) relaxation (see Table 1). using the following well-known relations:

$$\phi_{PL} = \frac{k_r}{k_r + k_{nr}}$$

$$\tau = \frac{1}{k_r + k_{nr}}$$

Altogether, k_r is of the same order of magnitude for all radicals (see Figure 6). By contrast, k_{nr} varies greatly and appears strongly reduced for the donor functionalized TBTM radicals compared to the TTM radical series. Therefore, k_{nr} appears to be the main descriptor of ϕ_{PL}, as indicated by the HR analysis, while the reduction of non-adiabatic coupling and suppressed exciton-phonon coupling in the D_2 state appear to be the main reason for the superior performance of the TBTM radicals over the TTM series. For all three TBTM radicals, we find much smaller k_{nr} as compared to the TTM series (see Figure 6).

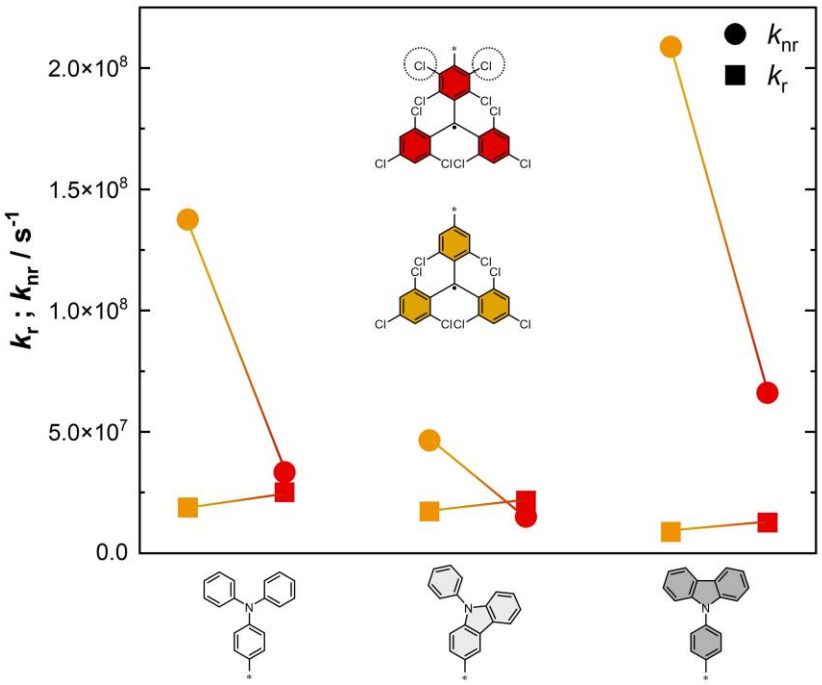

Figure 6: Rate constants of radiative (squares) and non-radiative (circles) relaxation for the different donor-functionalized radicals.

CONCLUSIONS

We have introduced a new series of donor-functionalized radicals by employing a TTM radical with two additional chlorine atoms in *meta*-position to the methine radical carbon. The additional chlorines apply steric constraints on the rotational freedom of the doner against the trityl radical acceptor. The donor and trityl moiety are forced into a close-to-perpendicular orientation, leading to a pronounced charge-separation in the excited state. We find highly improved values of ϕ_{PL} compared to the TTM reference series functionalized with identical donors by suppressing non radiative decay pathways. Our molecular design approach presents a new strategy in light emitting radicals to tune the optical properties, such as decay rates and ϕ_{PL}. In the future, this approach will allow the design and synthesis of highly efficient light emitting radicals with red-shifted emission into the near IR that could overcome the limits and restrictions imposed by the energy gap law.

AUTHOR INFORMATION

Corresponding Authors

* e-mail: alexander.kuehne@uni-ulm.de
* e-mail: koehn@theochem.uni-stuttgart.de
* e-mail: felix.deschler@pci.uni-heidelberg.de
* e-mail: mona.arnold@uni-ulm.de
†these authors contributed equally to this publication

ACKNOWLEDGMENTS

The authors acknowledge support by the state of Baden-Württemberg through bwHPC and the German Research Foundation (DFG) through grant no INST 40/575-1 FUGG (JUSTUS 2 cluster). We acknowledge funding by the

Deutsche Forschungsgemeinschaft (DFG, German Research Foundation) under project number: 500226157. Mona E. Arnold, Robert Toews, and Lars Schneider contributed equally to this work.

REFERENCES

[1] J. Ding, S. Dong, M. Zhang, F. Li, *J Mater Chem C Mater* **2022**, *10*, 14116–14121.

[2] J. M. Hudson, T. J. H. Hele, E. W. Evans, *J Appl Phys* **2021**, *129*, DOI 10.1063/5.0047636.

[3] C. He, Z. Li, Y. Lei, W. Zou, B. Suo, *Journal of Physical Chemistry Letters* **2019**, *10*, 574–580.

[4] A. Abdurahman, T. J. H. Hele, Q. Gu, J. Zhang, Q. Peng, M. Zhang, R. H. Friend, F. Li, E. W. Evans, *Nat Mater* **2020**, *19*, 1224–1229.

[5] H. H. Cho, S. Gorgon, G. Londi, S. Giannini, C. Cho, P. Ghosh, C. Tonnelé, D. Casanova, Y. Olivier, T. K. Baikie, F. Li, D. Beljonne, N. C. Greenham, R. H. Friend, E. W. Evans, *Nat Photonics* **2024**, DOI 10.1038/s41566-024-01458-3.

[6] Q. Peng, A. Obolda, M. Zhang, F. Li, *Angewandte Chemie International Edition* **2015**, *54*, 7091–7095.

[7] V. Gamero, D. Velasco, S. Latorre, F. López-Calahorra, E. Brillas, L. Juliá, *Tetrahedron Lett* **2006**, *47*, 2305–2309.

[8] L. Fajarí, R. Papoular, M. Reig, E. Brillas, J. L. Jorda, O. Vallcorba, J. Rius, D. Velasco, L. Juliá, *J Org Chem* **2014**, *79*, 1771–1777.

[9] L. Chen, M. Arnold, Y. Kittel, R. Blinder, F. Jelezko, A. J. C. Kuehne, *Adv Opt Mater* **2022**, *10*, DOI 10.1002/adom.202102101.

[10] P. Murto, B. Li, Y. Fu, L. E. Walker, L. Brown, A. D. Bond, W. Zeng, R. Chowdhury, H. H. Cho, C. P. Yu, C. P. Grey, R. H. Friend, H. Bronstein, *J Am Chem Soc* **2024**, *146*, 13133–13141.

[11] K. Nakamura, K. Matsuda, R. Xiaotian, M. Furukori, S. Miyata, T. Hosokai, K. Anraku, K. Nakao, K. Albrecht, *Faraday Discuss* **2023**, *250*, 192–201.

[12] M. E. Arnold, L. Roß, P. Thielert, F. Bartley, J. Zolg, F. Bartsch, L. A. Kibler, S. Richert, C. Bannwarth, A. J. C. Kuehne, *Adv Opt Mater* **2024**, DOI 10.1002/adom.202400697.

[13] S. Dong, W. Xu, H. Guo, W. Yan, M. Zhang, F. Li, *Physical Chemistry Chemical Physics* **2018**, *20*, 18657–18662.

[14] Z. Li, J. Wang, X. Liu, P. Gao, G. Li, G. He, B. Rao, *Angewandte Chemie International Edition* **2023**, *62*, DOI 10.1002/anie.202302835.

[15] C. Lu, E. Cho, K. Wan, C. Wu, Y. Gao, V. Coropceanu, J. L. Brédas, F. Li, *Adv Funct Mater* **2024**, DOI 10.1002/adfm.202314811.

[16] C. Wu, C. Lu, S. Yu, M. Zhang, H. Zhang, M. Zhang, F. Li, *Angewandte Chemie International Edition* **2024**, DOI 10.1002/anie.202412483.

[17] P. Ghosh, A. M. Alvertis, R. Chowdhury, P. Murto, A. J. Gillett, S. Dong, A. J. Sneyd, H. H. Cho, E. W. Evans, B. Monserrat, F. Li, C. Schnedermann, H. Bronstein, R. H. Friend, A. Rao, *Nature* **2024**, *629*, 355–362.

[18] C. Lu, E. Cho, Z. Cui, Y. Gao, W. Cao, J. L. Brédas, V. Coropceanu, F. Li, *Advanced Materials* **2023**, *35*, DOI 10.1002/adma.202208190.

[19] A. Heckmann, S. Dümmler, J. Pauli, M. Margraf, J. Köhler, D. Stich, C. Lambert, I. Fischer, U. Resch-Genger, *The Journal of Physical Chemistry C* **2009**, *113*, 20958–20966.

[20] M. E. Arnold, A. J. C. Kuehne, *Dyes and Pigments* **2023**, *208*, 110863.

[21] K. Matsuda, R. Xiaotian, K. Nakamura, M. Furukori, T. Hosokai, K. Anraku, K. Nakao, K. Albrecht, *Chemical Communications* **2022**, *58*, 13443–13446.

[22] T. Yanai, D. P. Tew, N. C. Handy, *Chem Phys Lett* **2004**, *393*, 51–57.

[23] E. Cho, V. Coropceanu, J. L. Brédas, *J Am Chem Soc* **2020**, *142*, 17782–17786.

[24] K. Huang, A. Rhys, *Proceedings of the Royal Society A* **1950**, *204*, 406–423.

[25] A. S. Bozzi, W. R. Rocha, *J Chem Theory Comput* **2023**, *19*, 2316–2326.

[26] L. Shi, X. Xie, A. Troisi, *Journal of Chemical Physics* **2022**, *157*, DOI 10.1063/5.0102857.

[27] J. S. Wilson, N. Chawdhury, M. R. A. Al-Mandhary, M. Younus, M. S. Khan, P. R. Raithby, A. Köhler, R. H. Friend, *J Am Chem Soc* **2001**, *123*, 9412–9417.

[28] E. Cho, V. Coropceanu, J. L. Brédas, *J Mater Chem C Mater* **2021**, *9*, 10794–10801.

[29] R. J. Cave, M. D. Newton, *Chem Phys Lett* **1996**, *249*, 15–19.

[30] R. Maksimenka, M. Margraf, J. Köhler, A. Heckmann, C. Lambert, I. Fischer, *Chem Phys* **2008**, *347*, 436–445.